ACCSCIENCE PUBLISHING

International Journal of Bioprinting

RESEARCH ARTICLE

Optimizing nozzle design in extrusion-based 3D bioprinting to minimize mechanical stress and enhance cell viability

Lorenzo Lombardi[1], Annachiara Scalzone[2,3]*, Chiara Ausilio[1], Piergiorgio Gentile[2,4]*, and Daniele Tammaro[1]

[1]Department of Chemical, Materials and Production Engineering, Polytechnic School and Basic Sciences, University of Naples Federico II, Naples, Campania, Italy

[2]School of Engineering, Faculty of Science, Agriculture and Engineering, Newcastle University, Newcastle upon Tyne, Tyne and Wear, United Kingdom

[3]Center for Advanced Biomaterials for Health Care, Italian Institute of Technology, Naples, Campania, Italy

[4]Center for Biomaterials and Tissue Engineering, Polytechnic University of Valencia, Valencia, Valencia, Spain

Abstract

Extrusion-based three-dimensional bioprinting is a widely used technique for fabricating cell-laden constructs in tissue engineering and regenerative medicine. However, the mechanical stresses experienced by cells during the printing process can negatively affect their viability. This study examines the influence of nozzle geometry—specifically contraction angle and outlet diameter—on stress distribution and its effects on cell survival. Through a combination of experimental analysis and theoretical modeling, the impacts of nozzle design on the balance between shear and extensional stresses during bioprinting are explored. The findings highlight the importance of optimizing nozzle parameters to minimize mechanical damage and enhance post-printing cell viability. The proposed model provides a framework for guiding nozzle design, offering insights into the development of customized bioprinting strategies that enhance construct fidelity and biological functionality. These results contribute to advancing bioprinting techniques for applications in tissue engineering and regenerative medicine.

Keywords: Customized nozzles; Extensional stress; Extrusion bioprinting

***Corresponding authors:**
Annachiara Scalzone (annachiara.scalzone@iit.it)

Piergiorgio Gentile (pgentil@upvnet.upv.es)

Citation: Lombardi L, Scalzone A, Ausilio C, Gentile P, Tammaro D. Optimizing nozzle design in extrusion-based 3D bioprinting to minimize mechanical stress and enhance cell viability. *Int J Bioprint*. 2025;11(4):315-327. doi: 10.36922/IJB025190182

Received: May 5, 2025
Revised: June 4, 2025
Accepted: June 16, 2025
Published online: June 16, 2025

Copyright: © 2025 Author(s). This is an Open Access article distributed under the terms of the Creative Commons Attribution License, permitting distribution and reproduction in any medium, provided the original work is properly cited.

Publisher's Note: AccScience Publishing remains neutral with regard to jurisdictional claims in published maps and institutional affiliations.

1. Introduction

Three-dimensional (3D) printing, also known as additive manufacturing or rapid prototyping, has been introduced since the late 1980s and provides a new paradigm for engineering design and manufacturing. This technique involves creating objects bottom-up by depositing material in a layer-by-layer pattern pre-designed in digital files, and, as a result, complex structures can be easily fabricated.[1] Over the past decades, additive manufacturing has been widely exploited in tissue engineering, giving rise to a specialized branch known as bioprinting, which integrates 3D printing

technology with cell biology and biomaterial science. This technology has revolutionized regenerative medicine by enabling the fabrication of complex, patient-specific tissues and organoids through the precise deposition of living cells, bioactive molecules, and extracellular matrix components.[2,3] The bioprinting technique is driven by the critical need to address significant challenges in regenerative medicine, particularly organ transplantation and tissue engineering.[4] Therefore, this approach not only offers a potential alternative to alleviate the organ shortage crisis[5] but also advances fields such as personalized medicine,[6] *in vitro* disease modeling, and high-throughput drug screening, offering sophisticated models that can better mimic human tissue architecture and function compared to conventional 2D cultures.[7]

Cell manipulation and deposition are fundamental to tissue engineering, prompting the development of various advanced methodologies to overcome associated challenges.[8] Human tissues exhibit a wide range of cellular densities, reflecting their diverse structures and functions. For example, native human tissues typically have a cell density of 1–3 billion cells per milliliter. This high cell density is essential for maintaining the complex architecture and functionality of various tissues.[9]

Several bioprinting techniques have been developed to process high-density cell-based bioinks. These include inkjet-based, laser-assisted, and extrusion-based bioprinting. Inkjet-based bioprinting, which relies on precise droplet deposition, is advantageous for its high resolution and ability to print multiple cell types simultaneously. However, it is limited by low cell density and potential nozzle clogging. Meanwhile, laser-assisted bioprinting offers superior resolution and cell viability by using laser pulses to transfer bioink onto a substrate; however, it requires complex setups and expensive materials. Among these, extrusion-based bioprinting remains the most scalable and adaptable method for fabricating large-scale tissue constructs with high cell density and structural integrity.[10]

Extrusion-based bioprinting operates by dispensing bioink—typically composed of living cells embedded in hydrogels—through a nozzle under applied pressure to create 3D constructs.[11] Common biomaterials used in this method include hydrogel-based inks, such as gelatin methacryloyl (GelMA), which is widely used due to its biocompatibility, tunable physicochemical properties, and ability to form stable hydrogels upon photo-cross-linking.[12] However, this technique requires highly viscous bioinks, which expose cells to significant mechanical stresses, particularly shear stress and extensional stress, that critically impact cell viability and post-printing function.[13,14] These mechanical forces can disrupt cell membranes, causing damage that adversely affects cell viability and, consequently, the functionality of the printed structures. Indeed, these stresses ultimately reduce cell viability to as low as 45%, depending on bioink viscosity, cell concentration, and nozzle diameter. During the printing process, shear stress primarily affects cells at the narrow tip of the needle.[15] In contrast, extensional stress occurs as cells pass through the constriction in the nozzle, where the channel narrows from the larger diameter of the syringe to the smaller diameter of the needle.[16]

Recent studies suggest that the extensional stress experienced by cells during the bioprinting process plays a significant role in cell membrane rupture, affecting their post-printing viability.[17,18] It is well-established that extensional flow is more effective than simple shear flow in deforming and disrupting droplets, bubbles, or vesicles.[19] Compared to shear stress, extensional stress is more likely to cause severe cell damage.[20,21] Despite this, most existing models of cell damage during bioprinting primarily focus on shear stress and do not adequately address the effects of extensional stress.[22] To fill this gap, Ning et al.[16] explored how both shear and extensional stresses generated during extrusion-based bioprinting contribute to cell damage. However, the role of nozzle design in influencing cell damage remains unexamined. Nozzle geometry, particularly contraction angle and final diameter, has the potential to modulate the relative contribution of shear and extensional stresses, thereby impacting cell viability.

This study hypothesizes that optimized nozzle design, specifically focusing on the contraction angle and final diameter, significantly enhances cell viability by reducing extensional stress during bioprinting. This work aims to investigate the feasibility of producing in-house nozzles that improve cell viability during the extrusion-based bioprinting process. Starting from the identification of a gap in bioprinting, represented by the lack of specific nozzles for different processes, tests were conducted to demonstrate the feasibility of performing a bioprinting process with custom-designed nozzles. Through a combination of simple analytical relationships and a computational cell damage model, a practical tool for optimizing nozzle design to minimize cell damage during the bioprinting process was proposed.

2. Materials and methods

2.1. Nozzle design and manufacturing

The 3D-printed nozzles for the bioprinter were produced using a stereolithography 3D printer (Anycubic Photon Mono X 6Ks, Anycubic, China) based on a digitally

designed model (Figure 1A). The fabricated nozzles are shown in Figure 1B, where their transparent structure enables visual inspection of their geometric accuracy.

Additionally, Figure 1B presents a longitudinally sectioned nozzle, providing a clear view of the internal channel and revealing any potential deviations from the intended geometry. To assess shape fidelity, the nozzle's internal structure was scanned using a confocal microscope (Leica DCM3D, Leica, Germany). The resulting 3D surface measurements are presented in Figure 1C and D, showing a tilted view and a top–down view, respectively. These scans offered accurate spatial data on the internal channel, facilitating the evaluation of manufacturing accuracy and identifying any deformations introduced during the 3D printing process.

A comparison of Figure 1A, B, and D demonstrates that the stereolithography-based 3D printing process achieved high shape fidelity. All nozzles included a converging section defined by a contraction angle (θ) and were further characterized by their inlet diameter (d_1), outlet diameter (d_2), and land length (LL). The values of these parameters for the nozzles fabricated and tested in this study are summarized in Table 1.

2.2. Cell culture

Human telomerase reverse transcriptase immortalized bone marrow stromal cell line Y201 was kindly supplied by Professor Paul Genever (University of York) at passage 84. The Y201 cells were cultured in Dulbecco's modified Eagle medium (DMEM, 1×) supplemented with 10% v/v fetal bovine serum (Sigma-Aldrich, USA) and 1% v/v

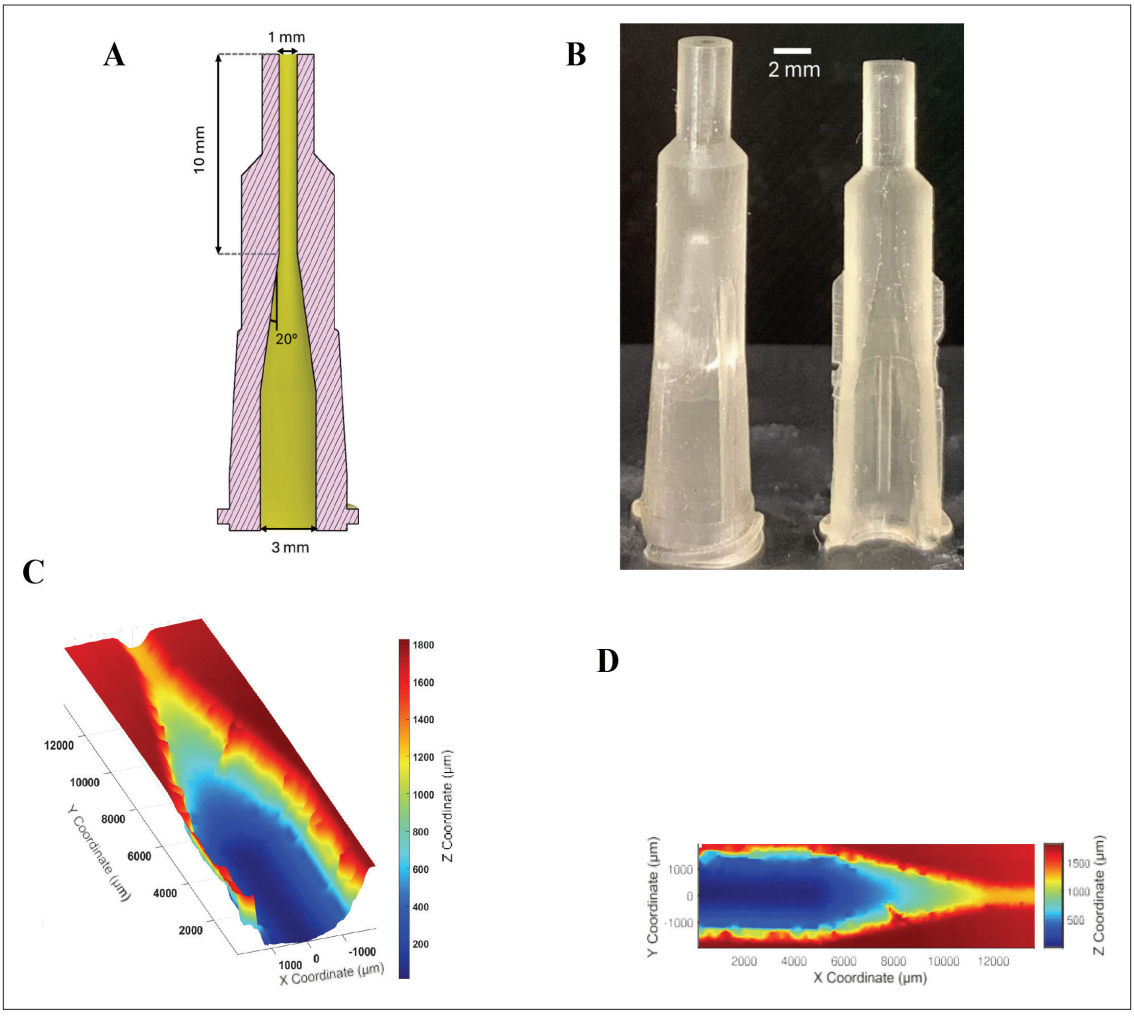

Figure 1. Designed nozzle analysis. (A) A cross-sectional image of the nozzle 3D model. (B) A 3D-printed nozzle model with a d_1 of 3 mm, d_2 of 1 mm, LL of 10 mm, and θ of 20°. (C & D) Confocal microscopy images of the nozzle interior reveal the internal surface topology and roughness, with the color scale representing height variations.

Table 1. Geometrical parameters for different nozzle configurations

d_1 (mm)	d_2 (mm)	LL (mm)	θ (°)
3	0.50	5	40, 80, 90
3	0.50	10	40, 80
3	0.75	5	40, 80, 90
3	0.75	10	40, 80, 90
3	1.00	5	40, 80, 90
3	1.00	10	40, 80

penicillin–streptomycin. The cells were maintained in a 5% CO_2, humidified incubator at 37°C. The Y201 cell line was selected for its reproducibility, robust growth, and common use in tissue engineering applications, including mechanobiology. Although the precise elastic modulus of Y201 cells has not been experimentally measured to date, an estimated value of 1000 Pa was used based on literature data for immortalized mesenchymal stromal cells under similar conditions. Before encapsulation in GelMA, the cells were detached by removing the culture medium and washing with 10 mL of phosphate-buffered saline (PBS). 3 mL of trypsin were added to facilitate detachment. Following incubation, 8 mL of fresh culture medium was added to neutralize the trypsin, and 10 mL of the cell suspension was transferred to a Falcon tube for centrifugation at 1200 rpm for 5 min. After centrifugation, the supernatant was discarded, and the cell pellet was resuspended in 10 mL of DMEM. Once counted, the cell suspension was divided into two separate flasks, and the volume was adjusted to 25 mL using culture medium to maintain appropriate cell density before GelMA encapsulation.

2.3. Gelatin methacrylate hydrogel synthesis

Type A gelatin derived from porcine skin (Sigma-Aldrich, USA) was dissolved in Dulbecco's PBS (DPBS, Gibco, USA) at 50°C to prepare a 10 wt.% uniform solution. Methacrylic anhydride (Sigma-Aldrich, USA) was added at a rate of 2 mL/min under continuous stirring to a final volume of 20 mL. The reaction was performed at 50°C for 3 h, ensuring thorough methacrylation of the gelatin. The resulting solution was then diluted 5× with additional warm DPBS (40°C) to reduce viscosity and facilitate purification. To remove unreacted methacrylic anhydride and by-products, the GelMA solution was dialyzed against deionized water using a 12–14 kDa cutoff dialysis tube for 3 d at 50°C. The purified GelMA was then frozen at −80°C, lyophilized, and stored at −80°C until further use. For cross-linking, a water-soluble photoinitiator, lithium phenyl(2,4,6-trimethylbenzoyl) phosphinate (Tokyo Chemical Industry, Japan), was used at a concentration of 5mg/mL. The GelMA constructs were exposed to ultraviolet light (405 nm, 10 mW/cm^2) for 15 s to initiate cross-linking.

2.4. Bioprinting procedure

Bioprinting was conducted using the Dr. INVIVO 4D2 bioprinter (Rokit Healthcare, Korea). Prior to printing, the syringe and bed temperatures were set to 25°C and 15°C, respectively, to maintain the bioink in a viscous state inside the syringe while ensuring optimal gelation on the printing bed (Table 2). A 9 cm-diameter Petri dish was placed on the bed surface, and the extruding syringe (BD Plastipak 10 mL Hypodermic Syringe, Becton Dickinson and Co., USA) was securely mounted in the extrusion unit. The bioprinter was then calibrated using its semi-automatic calibration system, following the on-screen instructions. The printing velocity was set to 5 mm/s, and with a 14 mm diameter syringe, this resulted in a flow rate (Q) of 7.7×10^{-7} m^3/s. The entire printing process was performed under sterile conditions. The bioprinter's chamber and bed were thoroughly disinfected with 70% isopropanol, and disposable 9 × 9 cm Petri dishes were used as printing substrates. To evaluate nozzle performance, multiple nozzles were tested by bioprinting a single drop. Following extrusion, each drop underwent photocuring at 405 nm, 10 mW/cm^2 for 15 s to initiate cross-linking (Figure 2).

2.5. Evaluation of cell viability and morphology

Cell viability was assessed using a Live/Dead kit (L3224, Thermo Fisher Scientific, UK), which combines Calcein-AM and ethidium bromide to provide two-color discrimination between live (green) and dead (red) cells. Samples were washed twice with DPBS before incubation with the staining solutions: 4 μM ethidium homodimer-1 and 10 μM calcein diluted in DPBS. Samples were incubated for 30 min at 37°C prior to fluorescence imaging using the EVOS M5000 Imaging System (Thermo Fisher Scientific, USA). Multiple images were obtained for each sample, and z-stacks were captured in three distinct regions of the samples. Z-projections were analyzed with Image-J software (NIH, USA). Each experimental trial was conducted in three replicates.

Table 2. Bioprinting parameters used in this study

Parameter	Value
Bed temperature	15 °C
Dispenser temperature	25 °C
Extrusion time	2 s
Printing velocity	5 mm/s
Extrusion height	0.5 mm

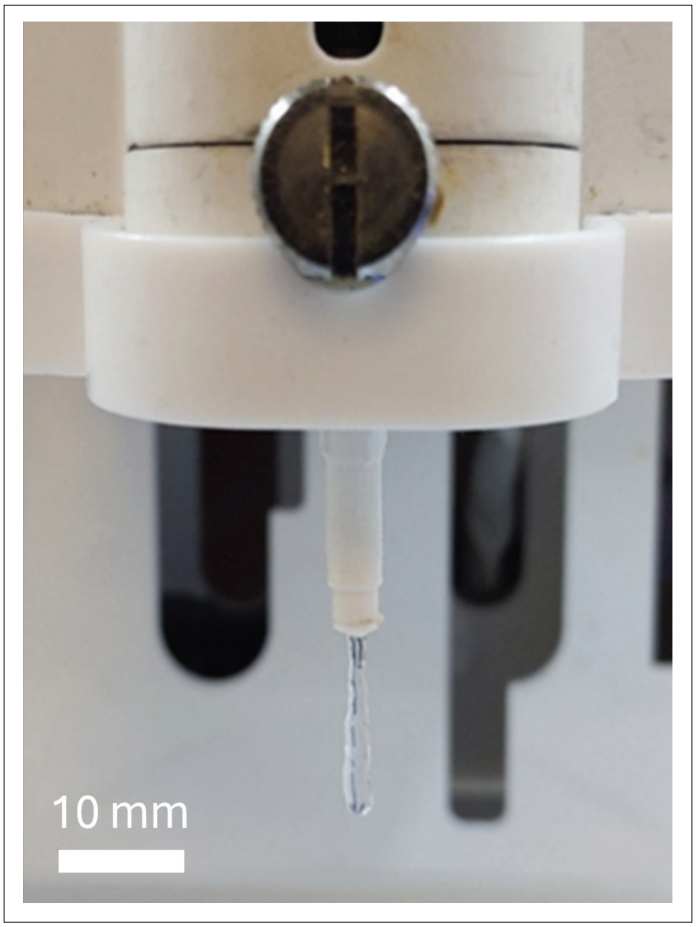

Figure 2. Close-up view of the 3D-printed bioprinter nozzle in operation, dispensing a bioink filament. The transparent nature of the nozzle allows for visual inspection of fluid extrusion.

3. Results and discussion

Extrusion-based bioprinting subjects cells to mechanical stresses, primarily shear stress along the nozzle walls and extensional stress in the contraction zone (Figure 3). While shear stress predominantly impacts cells at the narrow tip of the nozzle, extensional stress is more critical in causing cell damage as the bioink passes through the nozzle's contraction section. Recent studies highlight that extensional stress is often more detrimental than shear stress, as it induces membrane deformation, disrupts the cytoskeleton, and reduces cell viability.[16,22]

To investigate these effects, Y201 cell-loaded GelMA bioink was extruded through different nozzles, and cell viability was assessed 30 min post-printing. Live/dead staining and quantitative viability analysis revealed a consistent correlation between nozzle design and cell viability, highlighting the detrimental effect of larger contraction angles (Figure 4). Live cell counts indicated a higher concentration of viable cells (green) with a smaller nozzle contraction angle, whereas a greater number of dead cells (red) were observed with a larger contraction angle. This suggests that a larger contraction angle induces higher extensional stress, leading to increased cell damage. The elevated stress intensity at greater contraction angles aligns with theoretical models, which predict that wider contraction zones amplify extensional stress, particularly in highly viscous bioinks.[15] This intensified stress potentially contributed to localized membrane rupture and increased cellular damage.

To better interpret the findings and assess the significance of each stress contribution to cellular deformation and damage, a previously described approach was adopted.[16] According to the model, the fraction of dead cells resulting from shear stress at the needle tip is expressed as:

$$D_s = \frac{2\int_0^{\frac{d_2}{2}} r\left(1-e^{-a_1\sigma_s t_s}\right)dr}{d_2^2} \quad \text{(I)}$$

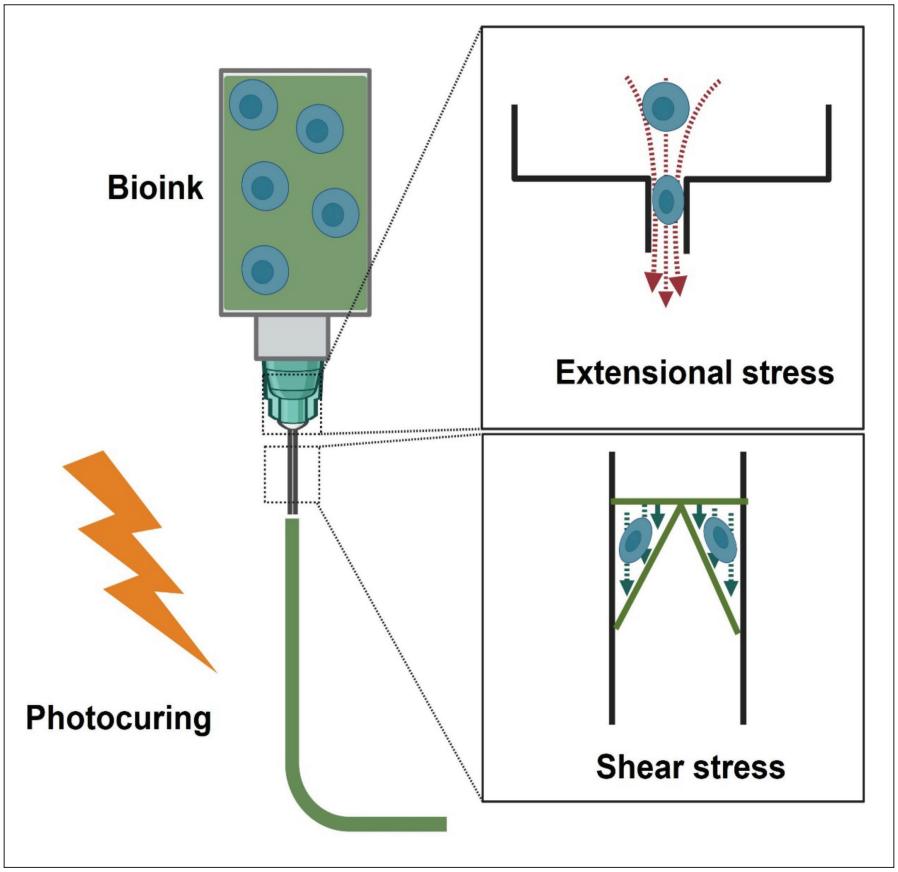

Figure 3. Schematic representation of the extrusion-based bioprinting process with 365 nm photocuring. During extrusion, the bioink undergoes extensional and shear stresses, affecting cellular behavior.

where σ_s is $\frac{\Delta P r}{2}$, representing the shear stress in the capillary after the converging section at a radial position $0 \le r \le d_2/2$. Here, L is the capillary length, and ΔP is the pressure drop in the capillary, which can be estimated using Poiseuille's law. The residence time of the cells in the capillary (t_s) is V_c/Q, where V_c is the volume of the cylindrical capillary, and Q is the volumetric flow rate.

In contrast, the damage to cells in the converging section is due to both extensional and shear stresses. The total pressure drop in the converging section can be expressed as:

$$P_c = P_{c,s} + P_{c,e} \quad \text{(II)}$$

where $P_{c,s}$ and $P_{c,e}$ are the pressure drops associated with shear and extensional flows, respectively.[23] According to Cogswell relations,[24] these components are given by:

$$P_s = \frac{2C\dot{\gamma}_c^n}{3n\tan\theta}\left[1-\left(\frac{d_2}{d_1}\right)^{3n}\right] \quad \text{(III)}$$

$$P_e = \eta\tan\theta\dot{\gamma}_c\left[1-\left(\frac{d_2}{d_1}\right)^{3}\right] \quad \text{(IV)}$$

where $\dot{\gamma}_c$ is calculated by $4Q/\pi(d_2/2)^3$, which is the shear rate, and C and n are the consistency index and power-law exponent of the fluid, respectively. A constant viscosity (η) of 0.15 Pa·s, was adopted for this analysis based on literature values obtained under matching GelMA concentration and temperature conditions.[25] The flow was approximated as Newtonian, with a flow behavior index (n) of 1. This assumption is supported by literature data indicating only weak shear-thinning behavior for GelMA under similar conditions; specifically, fitting of published rheological data yields a flow behavior index of approximately 0.92, validating the use of the Newtonian approximation in

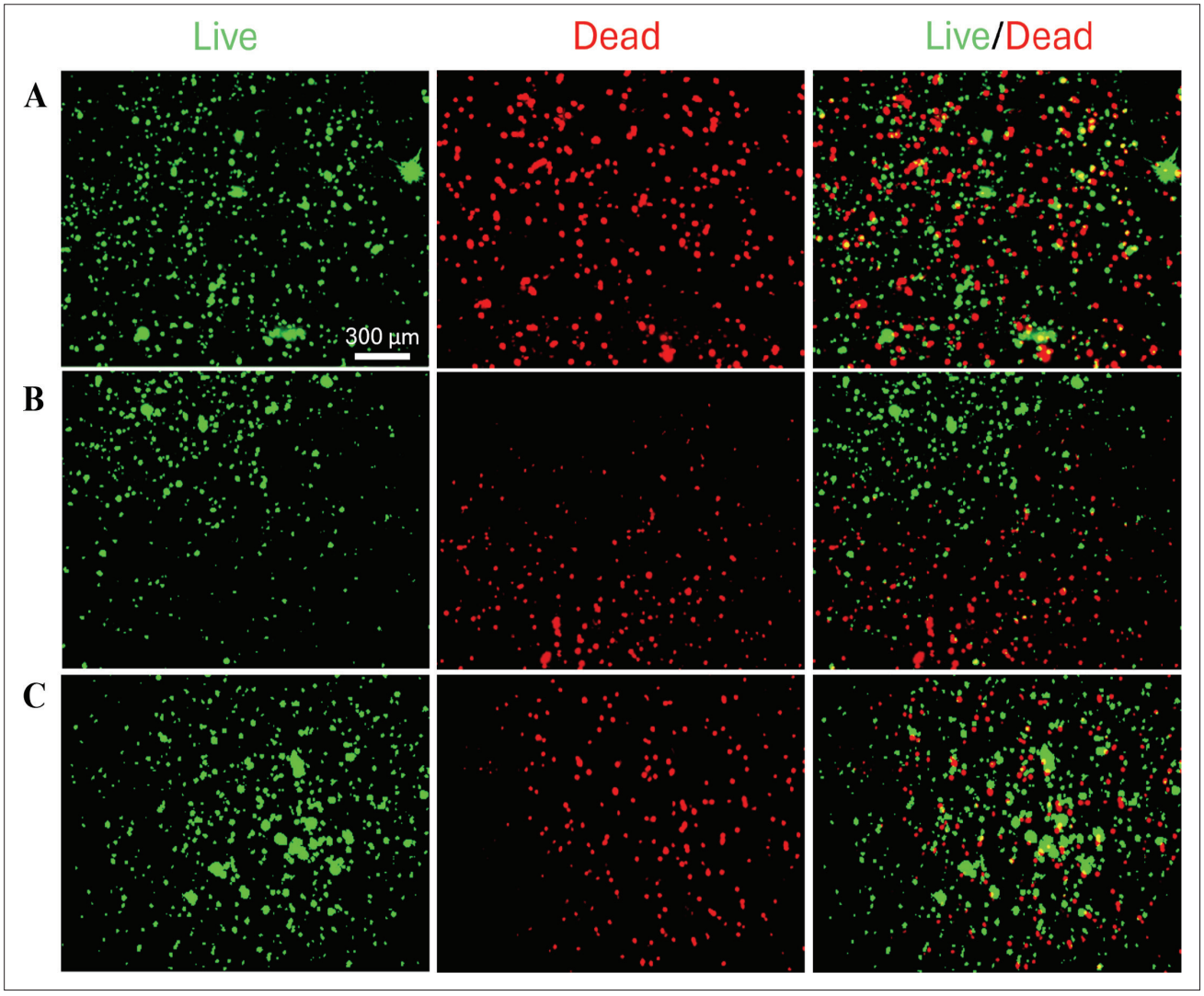

Figure 4. Cell viability assessment using Live/Dead staining 30 min after bioprinting. The images display live cells (green) and dead cells (red) following bioprinting with three different nozzle configurations: (A) d_1 = 3 mm, d_2 = 1 mm, LL = 5 mm, θ = 90°; (B) d_1 = 3 mm, d_2 = 1 mm, LL = 5 mm, θ = 80°; (C) d_1 = 3 mm, d_2 = 1 mm, LL = 5 mm, θ = 40°. Scale bar: 300 μm, magnification: 5×.

the current model. The average extensional stress in the converging section is given by[24]:

$$\sigma_e = (3/8)(n+1)P_c \quad \text{(V)}$$

Using this, the fraction of damaged cells due to extensional stress in the converging section can be expressed as[16]:

$$D_e = 1 - e^{-a_2\sigma_e} \quad \text{(VI)}$$

In **Equations I and VI**, the parameters a_1 and a_2 were obtained by fitting the model to experimental data. The overall fraction of damaged cells in the nozzle is expressed as[16]:

$$D_t = D_e + (1 - D_e)D_s \quad \text{(VII)}$$

Figure 5 demonstrates the fraction of dead cells (D_t) as a function of θ in the nozzle of a 3D bioprinter. Each plot corresponds to a unique combination of d_1, d_2, and LL. The experimental results reveal a clear dependence of D_t on θ, with D_t increasing with θ, and a minimal cell death was observed when θ was 40°. This trend is consistent

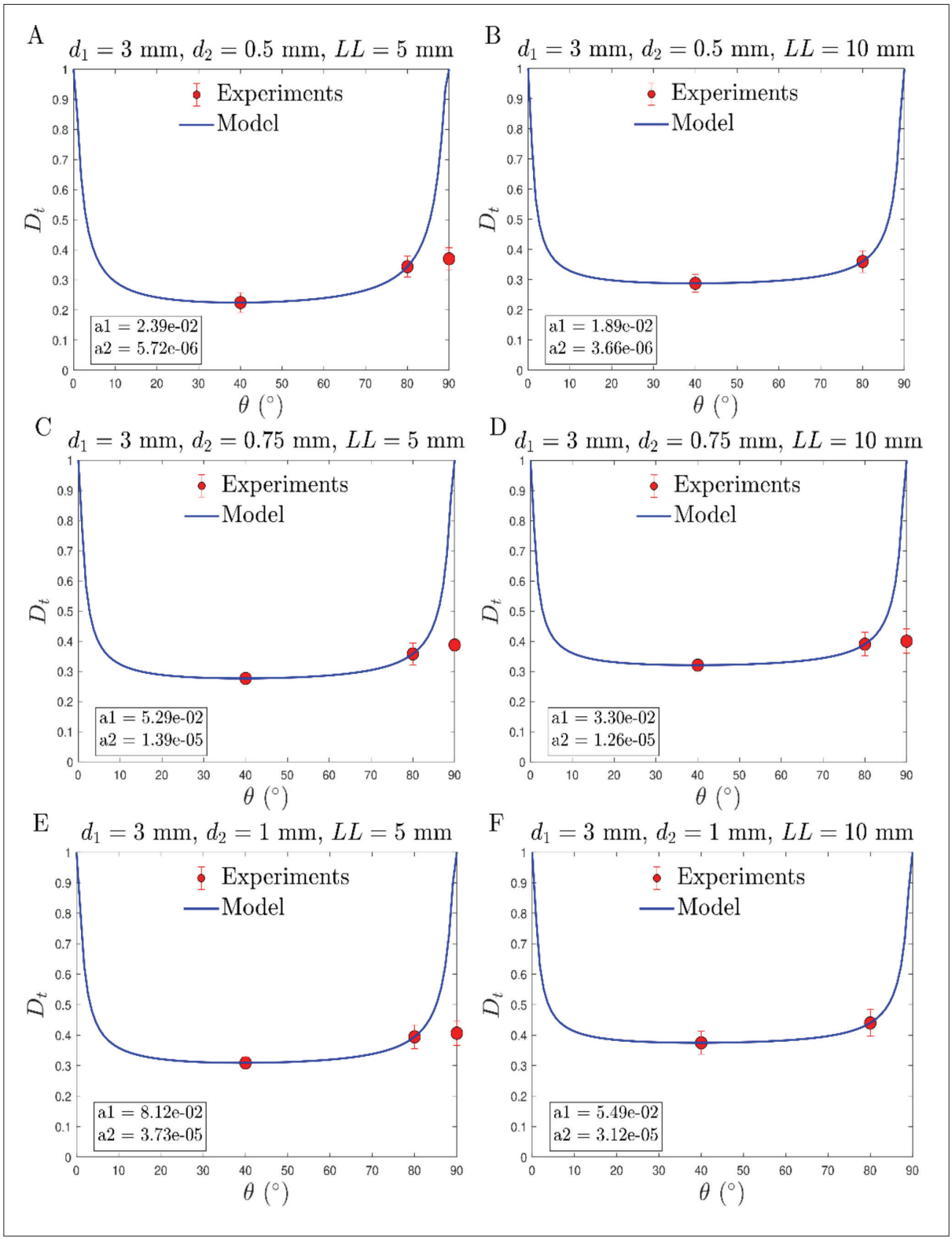

Figure 5. Comparison between experimental data and model predictions for the fraction of damaged cells (D_t) as a function of the converging section angle (θ). Each subplot corresponds to different nozzle geometries with a fixed inlet diameter ($d_1 = 3$ mm): (A) $d_2 = 0.5$ mm, $LL = 5$ mm; (B) $d_2 = 0.5$ mm, $LL = 10$ mm; (C) $d_2 = 0.75$ mm, $LL = 5$ mm; (D) $d_2 = 0.75$ mm, $LL = 10$ mm; (E) $d_2 = 1.0$ mm, $LL = 5$ mm; (F) $d_2 = 1.0$ mm, $LL = 10$ mm.

across all geometric configurations. The effects of d_2 and LL were also apparent in the plots. Increasing d_2 (from 0.5 to 1 mm) generally led to a higher D_t. Similarly, increasing LL (from 5 to 10 mm) enhanced D_t, particularly at larger angles, potentially due to prolonged exposure to stress in the longer capillary.

When comparing subplots Figure 5A and B, the effect of increasing LL from 5 to 10 mm at a fixed d_2 of 0.5 mm becomes evident, with cell damage increasing significantly at higher θ. Similarly, comparing Figure 5A and C at a fixed LL of 5 mm and increasing d_2 from 0.5 to 0.75 mm, a moderate increase in cell damage was observed, highlighting the interplay between d_2 and θ. This comparative trend remains consistent across other geometries.

The model (**Equation VII**) predicted a non-monotonic relationship between D_t and θ. Across all geometric configurations, minimal cell death was predicted at intermediate angles ($\theta \approx 30$–$60°$), whereas extreme angles ($\theta \to 0°$ and $\theta \to 90°$) resulted in significantly higher D_t. This behavior is attributed to the combined effects of shear and extensional stress. At small angles, cells were subjected to prolonged shear and extensional stress within the converging section. As $\theta \to 0°$, the length and volume of the converging section diverge, leading to a sharp increase in cell death. Conversely, at large angles, the abrupt contraction induced significant extensional stress, which damaged the cells. The analytical model predicted a diverging D_t as $\theta \to 90°$.

Deviations between the experimental data and the model were observed when θ is 90°, potentially due to unaccounted factors in the analytical model, such as the intrinsic resistance of cells to deformation. These discrepancies highlight the complexity of the underlying mechanisms and suggest potential areas for improvement in the model.

The observed increase in cell death with increasing LL can be intuitively explained by the combined effects of increased shear stress and prolonged stress duration, as a longer LL provides more time for cells to experience flow-induced stresses. However, the decrease in D_t observed at smaller capillary diameters may appear counterintuitive (Figure 6). One would expect that, as the capillary diameter decreases, the shear stress increases significantly, resulting in higher cell damage. This observation suggests that the duration of exposure to shear stress may play a more critical role than the magnitude of the shear stress in determining D_t.

To assess the relative importance of shear stress, extensional stress, and t_s, it is convenient to introduce three non-dimensional parameters that incorporate the fluid properties and geometrical parameters varied in this study. From a physical perspective, when considering cells as elastic particles, the elastic capillary number, Ca_e, emerges as a key parameter in characterizing their behavior under

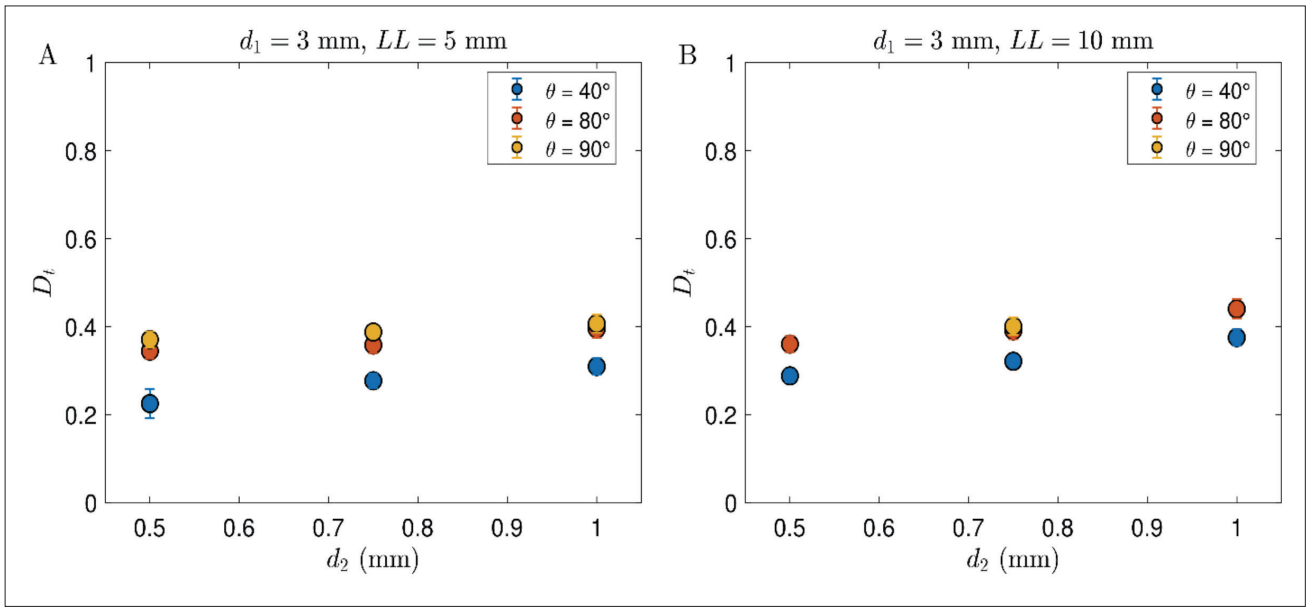

Figure 6. Fraction of damaged cells (D_t) as a function of the outlet diameter (d_2) for different converging section angles (θ). (A) LL = 5 mm. (B) LL = 10 mm.

flow conditions.[26] This dimensionless number quantifies the relative importance of fluid viscous stresses compared to the elastic stresses of the particle. The expression for Ca_e depends on the type of flow. For example, in extensional flow, it is defined as:

$$Ca_e = \eta \dot{\epsilon} / G \quad \text{(VIII)}$$

where G is the elastic modulus of the cell, and $\dot{\epsilon}$ is the elongation rate.

Literature values, supported by compression tests on immortalized human mesenchymal stem cells at similar temperatures,[27,28] indicate an elastic modulus of approximately 1000 Pa for Y201 cells, which was used in this analysis. While this value is an approximation due to the lack of specific mechanical characterization of Y201 cells in the literature, it provides a reasonable estimate for calculating dimensionless capillary numbers. In the case of shear flow, the Ca_e becomes:

$$Ca_s = \eta \dot{\gamma} / G \quad \text{(IX)}$$

where $\dot{\gamma}$ is the shear rate.

In the present study, both types of flow—extensional and shear flows—are encountered. Additionally, a non-dimensional residence time, τ_s, can be defined as:

$$\tau_s = t_s / t_c \quad \text{(X)}$$

where t_s is the actual residence time in the capillary and t_c is calculated by η/G, representing the characteristic timescale of the system.

The fraction of damaged cells can be effectively visualized as a function of the non-dimensional parameters described earlier, as shown in Figure 7A. Data corresponding to a 90° contraction angle was excluded from the analysis because, in this scenario, $Ca_e \to \infty$. In this plot, the color gradient represents the τ_s, and the planes were generated by

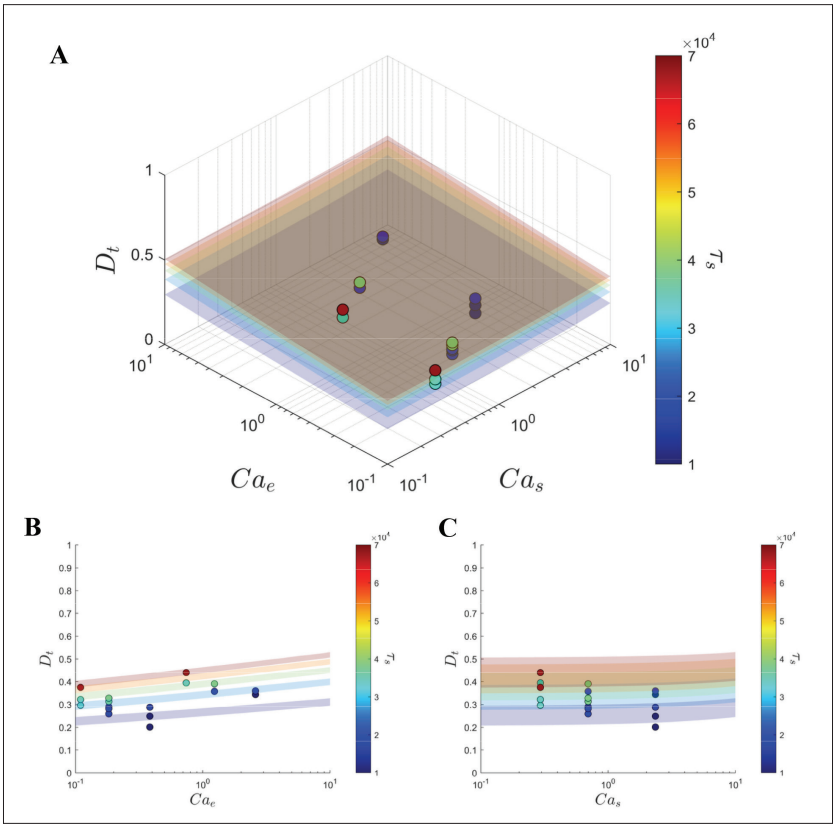

Figure 7. Fraction of damaged cells (D_t) as a function of the elastic capillary numbers in extensional (Ca_e) and shear (Ca_s) flows, with non-dimensional residence time (τ_s) represented by the color scale. (A) A 3D surface plot illustrating the relationship between D_t, Ca_s, and Ca_e, with experimental data points color-coded according to τ_s. (B) A 2D projection of D_t vs. Ca_e, showing how cell damage increases with extensional flow effects. (C) A 2D projection of D_t vs. Ca_s, highlighting the influence of shear flow on cell damage. The colored planes represent fits to experimental data using **Equations XI** and **XII**. The obtained fitting parameters are: $a = 0.0100$, $b = 0.0100$, $c = 0.7000$, $d = 0.0892$, and $e = 0.3629$.

fitting a modified expression for cell damage under shear and extensional stresses. These expressions consider an exponential dependence on Ca_e, Ca_s, and τ_s:

$$D_s = 1 - e^{-aCa_s^b \tau_s^c} \quad \text{(XI)}$$

$$D_e = 1 - e^{-dCa_e^e} \quad \text{(XII)}$$

where a, b, c, d, and e are fitting parameters determined by fitting **Equations XI and XII** to all experimental data.

As illustrated in Figure 7B, an increase in Ca_e resulted in a higher D_t for a given τ_s. This is consistent with the understanding that higher values of Ca_e correspond to greater cell deformation in extensional flows, leading to increased cell damage. The color gradient representing τ_s further highlights that lower residence times are associated with reduced fractions of damaged cells.

In Figure 7A, the effect of increasing τ_s is apparent, with transitions between nearly parallel planes in the parameter space of Ca_e, Ca_s, and τ_s. Conversely, the impact of shear stress was significantly less pronounced, as shown in Figure 7C. The data reveal a weak dependence of D_t on Ca_s for a given τ_s. However, an increase in τ_s still leads to a notable increase in cell damage. This weak correlation between D_t and Ca_s can explain the observed behavior of D_t with varying d_2, as seen in Figure 5. A reduction in d_2 increases Ca_s and, consequently, the shear stress. However, this increase in shear stress is relatively ineffective in deforming and damaging cells, as shown in Figure 7C. Simultaneously, a decrease in d_2 reduces the residence time in the capillary, thereby limiting the exposure of cells to shear stress and ultimately reducing cell damage.

The non-linear dependence of cell deformability on Ca_e, Ca_s, and τ_s is highly influenced by the specific response of cells to these flow conditions, making accurate modeling challenging. The introduction of fitting parameters helps address this complexity. Notably, the greater effectiveness of extensional flows in deforming particles compared to shear flows has been previously highlighted by Grace,[19] also emphasizing the importance of exposure time to shear conditions in determining particle deformation.

4. Conclusion

This study comprehensively examines the influence of nozzle design on cell viability in extrusion-based 3D bioprinting. Through experimental observations and theoretical modeling, it is demonstrated that nozzle geometry—particularly θ and d_2—plays a critical role in modulating mechanical stresses that affect cells. Optimizing these parameters can minimize extensional stress, thereby improving post-printing viability.

The findings indicate that extensional stress, rather than shear stress, is a primary cause of cell damage, particularly in the contraction region of the nozzle. Based on the results, it is recommended that nozzle designs with intermediate θ (30–60°) be used to balance extensional and shear stresses, thus optimizing cell viability. Furthermore, reducing capillary length and d_2 can decrease exposure time to mechanical stress, thereby improving cell survival. These parameters should be prioritized when designing nozzles for sensitive or high-density cell bioinks.

The proposed model helps to understand the relationship between nozzle geometry and stress-induced cellular damage, offering another perspective that can guide future nozzle designs to improve bioprinting results. From an application standpoint, engineering customized nozzles with optimized geometries holds great promise for enhancing bioprinting outcomes, ultimately advancing regenerative medicine and tissue engineering. The findings from this study provide critical insights that can inform the design of next-generation bioprinters capable of producing high-fidelity, cell-rich constructs with enhanced biological functionality.

In conclusion, this study highlights the crucial role of nozzle design in bioprinting. By systematically refining nozzle geometry, it can reduce mechanical stress, enhance cell viability, and improve the overall quality of bioprinted tissues, bringing bioprinting closer to clinical applications in regenerative medicine. With the rise of innovative bioprinting techniques—such as printing within a self-healing support bath that can be subsequently washed away to enable the fabrication of complex structures—it would be highly beneficial to develop long needles capable of penetrating deeply into the support material. Long needles—whose extended capillary length could increase cell exposure to mechanical stress—are increasingly necessary for support-bath-based printing strategies. The current findings on the role of needle length offer a valuable starting point for optimizing such designs.

Acknowledgments

None.

Funding

None.

Conflict of interest

The authors declare they have no competing interests.

Author contributions

Conceptualization: Annachiara Scalzone, Piergiorgio Gentile, Daniele Tammaro
Formal analysis: Lorenzo Lombardi
Investigation: Lorenzo Lombardi, Annachiara Scalzone, Chiara Ausilio
Methodology: All authors
Writing–original draft: Lorenzo Lombardi, Annachiara Scalzone, Chiara Ausilio
Writing–review & editing: Piergiorgio Gentile, Daniele Tammaro

Ethics approval and consent to participate

Not applicable.

Consent for publication

Not applicable.

Availability of data

Data are available upon request via lorenzo.lombardi@unina.it and annachiara.scalzone@iit.it.

References

1. Jim´enez M, Romero L, Dom´ınguez IA, Espinosa MdM, Dom´ınguez M. Additive manufacturing technologies: an overview about 3D printing methods and future prospects. *Complexity.* 2019;2019:9656938. doi: 10.1155/2019/9656938
2. Gu BK, Choi DJ, Park SJ, Kim MS, Kang CM, Kim CH. 3-Dimensional bioprinting for tissue engineering applications. *Biomater Res.* 2016;20(1):1–8. doi: 10.1186/s40824-016-0058-2
3. Jose RR, Rodriguez MJ, Dixon TA, Omenetto F, Kaplan DL. Evolution of bioinks and additive manufacturing technologies for 3D bio-printing. *ACS Biomater Sci Eng.* 2016;2(10):1662–1678. doi: 10.1021/acsbiomaterials.6b00088
4. Bertassoni LE, Bertassoni LE. Bioprinting of complex multicellular organs with advanced functionality—recent progress and challenges ahead. *Adv Mater.* 2022; 34(3):2101321. doi: 10.1002/ADMA.202101321
5. Parihar A, Pandita V, Kumar A, et al. 3D printing: advancement in biogenerative engineering to combat shortage of organs and bioapplicable materials. *Regen Eng Transl Med.* 2021;8:173–199. doi: 10.1007/S40883-021-00219-W
6. Lam EHY, Yu F, Zhu S, Wang Z. 3D bioprinting for next-generation personalized medicine. *Int J Mol Sci.* 2023;24(7):6357. doi: 10.3390/IJMS24076357
7. Mazzocchi A, Soker S, Skardal A. 3D bioprinting for high-throughput screening: drug screening, disease modeling, and precision medicine applications. *Appl Phys Rev.* 2019;6:1–12. doi: 10.1063/1.5056188
8. Chen A, Wang W, Mao Z, et al. Multimaterial 3D and 4D bioprinting of heterogenous constructs for tissue engineering. *Adv Mater.* 2024;36(34):2307686. doi: 10.1002/adma.202307686
9. You S, Xiang Y, Hwang HH, et al. High cell density and high-resolution 3D bioprinting for fabricating vascularized tissues. *Sci Adv.* 2023;9(8):eade7923. doi: 10.1126/sciadv.ade7923
10. Scalzone A, Tonda-Turo C, Ferreira AM, Gentile P. 3D-printed soft hydrogels for cell encapsulation. In: Azevedo HS, Mano JF, Borges J, eds. *Soft Matter for Biomedical Applications.* Royal Society of Chemistry. London, UK; 2021:594–625. doi: 10.1039/9781839161124-00594. Soft Matter Series.
11. Levato R, Jungst T, Scheuring RG, Blunk T, Groll J, Malda J. From shape to function: the next step in bioprinting. *Adv Mater.* 2020;32(12):1906423. doi: 10.1002/adma.201906423
12. Ying G, Jiang N, Yu C, Zhang YS. Three-dimensional bioprinting of gelatin methacryloyl (GelMA). *Bio Des Manuf.* 2018;1:215–224. doi: 10.1007/S42242-018-0028-8
13. Pedde RD, Mirani B, Navaei A, et al. Emerging biofabrication strategies for engineering complex tissue constructs. *Adv Mater.* 2017;29(19):1606061. doi: 10.1002/adma.201606061
14. Tian X, Li M, Chen X. Bio-rapid-prototyping of tissue engineering scaffolds and the process-induced cell damage. *J Biomim Biomater Tissue Eng.* 2013;17:1–23. doi: 10.4028/www.scientific.net/JBBTE.17.1
15. Lucas L, Aravind A, Emma P, Christophe M, Edwin-Joffrey C. Rheology, simulation and data analysis toward bioprinting cell viability awareness. *Bioprinting.* 2021;21:e00119. doi: 10.1016/J.BPRINT.2020.E00119
16. Ning L, Betancourt N, Schreyer DJ, Chen X. Characterization of cell damage and proliferative ability during and after bioprinting. *ACS Biomater Sci Eng.* 2018;4(11):3906–3918. doi: 10.1021/acsbiomaterials.8b00714
17. Bae YB, Jang HK, Shin TH, et al. Microfluidic assessment of mechanical cell damage by extensional stress. *Lab Chip.* 2016;16(1):96–103. doi: 10.1039/C5LC01006C
18. Ning L, Chen X. A brief review of extrusion-based tissue scaffold bio-printing. *Biotechnol J.* 2017;12(8):1600671. doi: 10.1002/BIOT.201600671

19. Grace HP. Dispersion phenomena in high viscosity immiscible fluid systems and application of static mixers as dispersion devices in such systems. *Chem Eng Commun.* 1982;14(3-6):225–277.
doi: 10.1080/00986448208911047

20. Aguado BA, Mulyasasmita W, Su J, Lampe KJ, Heilshorn SC. Improving viability of stem cells during syringe needle flow through the design of hydrogel cell carriers *Tissue Eng Part A.* 2012;18(7-8):806–815.
doi: 10.1089/TEN.TEA.2011.0391

21. Down LA, Papavassiliou DV, O'Rear EA. Significance of extensional stresses to red blood cell lysis in a shearing flow. *Ann Biomed Eng.* 2011;39:1632–1642.
doi: 10.1007/S10439-011-0262-0

22. Boularaoui S, Al Hussein G, Khan KA, Christoforou N, Stefanini C. An overview of extrusion-based bioprinting with a focus on induced shear stress and its effect on cell viability. *Bioprinting.* 2020;20:e00093.
doi: 10.1016/J.BPRINT.2020.E00093

23. Cogswell FN. Measuring the extensional rheology of polymer melts. *Trans Soc Rheol.* 1972;16(3):383–403.
doi: 10.1122/1.549257

24. Cogswell FN. Converging flow of polymer melts in extrusion dies. *Polym Eng Sci.* 1972;12(1):64–73.
doi: 10.1002/PEN.760120111

25. Alam K, Iqbal M, Hasan A, Al-Maskari N. Rheological characterization of biological hydrogels in aqueous state. *J Appl Biotechnol Rep.* 2020;7(3):171–175.
doi: 10.30491/JABR.2020.109994

26. Villone MM, Maffettone PL. Dynamics, rheology, and applications of elastic deformable particle suspensions: a review. *Rheol Acta.* 2019;58:109–130.
doi: 10.1007/S00397-019-01134-2

27. Tan SCW, Pan WX, Ma G, Cai N, Leong KW, Liao K. Viscoelastic behaviour of human mesenchymal stem cells. *BMC Cell Biol.* 2008;9(9):40.
doi: 10.1186/1471-2121-9-40

28. Nikolaev NI, Mu¨ller T, Williams DJ, Liu Y. Changes in the stiffness of human mesenchymal stem cells with the progress of cell death as measured by atomic force microscopy. *J Biomech.* 2014;47(3):625–630.
doi: 10.1016/j.jbiomech.2013.12.004